

Expression of 24,426 human alternative splicing events and predicted *cis* regulation in 48 tissues and cell lines

John C Castle¹, Chaolin Zhang², Jyoti K Shah¹, Amit V Kulkarni¹, Auinash Kalsotra³, Thomas A Cooper^{3,4} & Jason M Johnson¹

Alternative pre-messenger RNA splicing influences development, physiology and disease, but its regulation in humans is not well understood, partially because of the limited scale at which the expression of specific splicing events has been measured. We generated the first genome-scale expression compendium of human alternative splicing events using custom whole-transcript microarrays monitoring expression of 24,426 alternative splicing events in 48 diverse human samples. Over 11,700 genes and 9,500 splicing events were differentially expressed, providing a rich resource for studying splicing regulation. An unbiased, systematic screen of 21,760 4-mer to 7-mer words for *cis*-regulatory motifs identified 143 RNA 'words' enriched near regulated cassette exons, including six clusters of motifs represented by UCUCU, UGCAUG, UGCU, UGUGU, UUUU and AGGG, which map to *trans*-acting regulators PTB, Fox, Muscleblind, CELF/CUG-BP, TIA-1 and hnRNP F/H, respectively. Each cluster showed a distinct pattern of genomic location and tissue specificity. For example, UCUCU occurs 110 to 35 nucleotides preceding cassette exons upregulated in brain and striated muscle but depleted in other tissues. UCUCU and UGCAUG seem to have similar function but independent action, occurring 5' and 3', respectively, of 33% of the cassette exons upregulated in skeletal muscle but co-occurring for only 2%.

Alternative splicing is a key mechanism for generating proteomic diversity, and as many as 74% of human multi-exon genes are alternatively spliced¹. Many recent studies point to the importance of detection and measurement of alternative splicing. For example, more genetic variations in the CEU HapMap population manifest themselves through changes in transcript structure, including splicing, than changes in gene transcription². However, our knowledge of the differential expression of specific splicing events and characterization of corresponding *cis*-regulatory elements is limited. Likewise, although sequence targets of several individual RNA-binding splicing factors have been characterized, much remains to be learned about their regulatory mechanism within different human tissues.

PTB proteins are known to interact with pyrimidine-rich elements, such as UCUCU³⁻⁵; the FOX proteins bind UGCAUG^{6,7}; hnRNP A/B and hnRNP F/H bind GGGG and AGGGG, respectively, and GGG^{8,9}; muscleblind (MBNL) proteins bind UGCU¹⁰; TIA-1 binds U-rich sequences¹¹; and the CELF proteins¹² and SUP-12 (RBM38)^{12,13} interact with UGUGU. Using microarrays¹⁴ and immunoprecipitation of cross-linked RNA¹⁵, a previous study elucidated the binding element and regulatory influence of neuronal Nova RNA-binding proteins, showing that Nova binds either YCAY or YCATY (Y, pyrimidine), and causes exon inclusion or exclusion depending on the location of the motif relative to the exon.

Assessing the ratios of expression for two mutually exclusive splice forms ('splicing-event profiling') requires probes targeting both exons and junctions, for example, probes monitoring both the cassette exon and the junction across the excluded exon. Pan *et al.*¹⁶ (3,100 cassette exons, 10 tissues), Fagnani *et al.*¹⁷ (3,700 cassette exons, 27 tissues) and Sugnet *et al.*¹⁸ (6,700 events, 22 tissues) have previously used such arrays to profile mouse tissues. To further our understanding of alternative splicing expression and regulation, we generated the first human genome-wide alternative splicing-event compendium, monitoring 24,426 events in 48 tissues and cell lines, and undertook an unbiased, systematic search to identify and describe putative regulatory motifs.

RESULTS

Microarrays for whole-transcript profiling

We designed microarrays monitoring 203,672 exons and 178,351 exon-exon junctions in 17,939 human genes. These microarrays report expression of both splicing event isoforms from 8,000 cassette exons, 3,950 alternative 5' splice sites, 3,672 alternative 3' splice sites, 3,770 multiple cassette exons, 3,123 mutually exclusive exons and 1,890 inserted introns. The 'whole transcript' design used here is different from exon arrays¹⁹, junction arrays¹ and cassette exon-splicing arrays¹⁶ in that it includes a constellation of probes targeting every exon and every junction, similar to the approach of Griffith

¹Rosetta Inpharmatics LLC, Seattle, Washington 98109, USA. ²Cold Spring Harbor Laboratory, 1 Bungtown Road, Cold Spring Harbor, New York 11724, USA.

³Departments of Pathology and ⁴Molecular and Cellular Biology, Baylor College of Medicine, Houston, Texas 77030, USA. Correspondence should be addressed to J.C.C. (john_castle@merck.com) or J.M.J. (jason_johnson@merck.com).

Received 4 June; accepted 25 September; published online 2 November 2008; doi:10.1038/ng.264

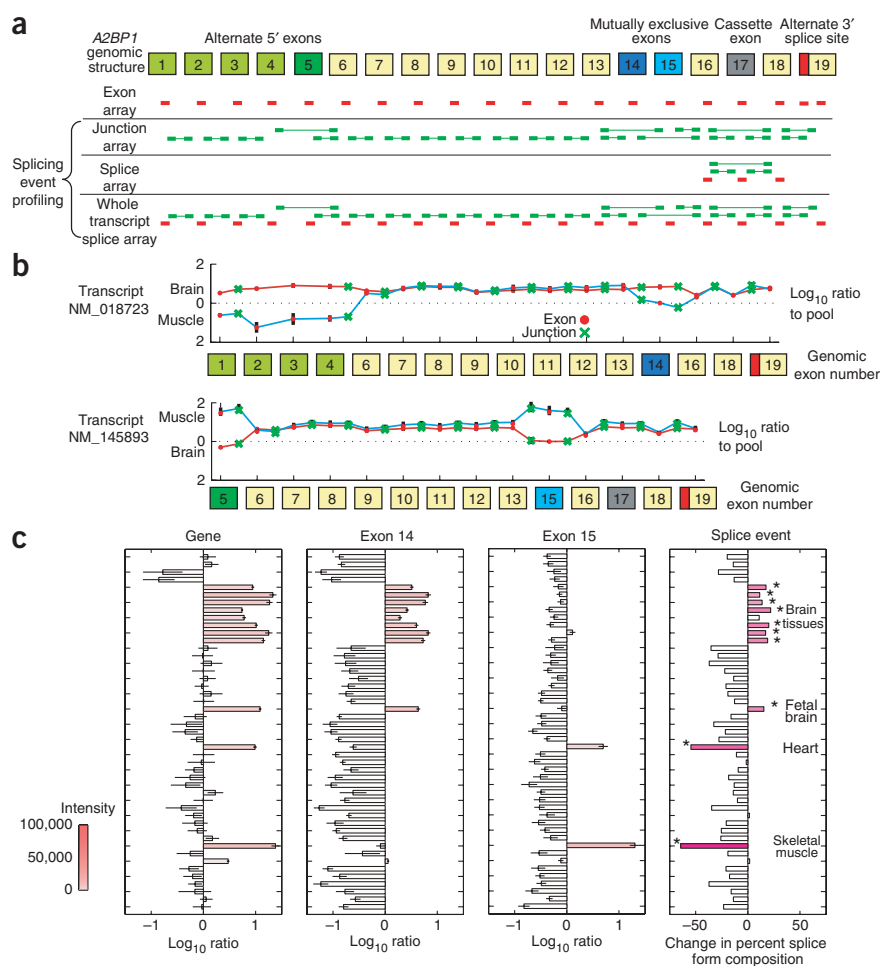


Figure 1 Interrogation of A2BP1 (Fox-1) isoforms on the alternative splicing microarrays. **(a)** The 19 exons in the locus, including alternative 5' exons (green), mutually exclusive exons (blue), a cassette exon (gray), and an alternative 3' splice site (red). Exon (red) and exon–exon junction (green) probes are shown for several splice-related microarrays. **(b)** Expression (\log_{10} change relative to reference pool) of exons (red dots) and junctions (green crosses) in transcripts NM_018723 and NM_145893 in skeletal muscle (cyan line) and brain (red line). **(c)** Expression of the gene, exon 15, exon 14 and the combined splice-event expression level. Red shading represents microarray intensity values; dark pink shading (right) represents more significant P values. Error bars for \log_{10} ratios represent expression uncertainties (Methods). Samples are ordered alphabetically as in **Figure 2**.

*et al.*²⁰ (**Fig. 1a**). Although exon arrays provide an unbiased survey of transcript structure, they do not monitor connections between individual exons or many alternative 5' and 3' splice sites. Because they lack junction probes, they also generally monitor only one form of an alternative splicing event. The inability to monitor both of the two mutually exclusive forms prevents accurate measurement of expression ratios of the two forms. Cassette exon splicing arrays, with probes designed to monitor the inclusion and exclusion of known cassette exons, are an economical option for profiling cassette exon splicing events but lack probes to profile other types of alternative splicing (for example, alternative 5' and 3' splice sites), do not monitor alternative 5' and 3' exons, and do not permit discovery of new alternative splice forms.

Compendium of human alternative splicing events

A set of 48 human tissues and cell lines with dissimilar expression patterns was hybridized to the arrays, and 11,700 of 18,000 genes monitored by the array showed greater than threefold

change in gene expression relative to the pool ($P < 0.01$) in at least one tissue (Methods and **Supplementary Fig. 1** online). Across the 48 tissue panel, 9,516 alternative splicing events were also significantly differentially expressed in at least one tissue (Methods and **Supplementary Fig. 2** online), similar to the number of differentially expressed genes.

As an example of the data available for each gene, results for A2BP1 (Fox-1) are shown in **Figure 1**. A2BP1 regulates alternative splicing and is itself alternatively spliced, containing alternative 5' exons, a pair of mutually exclusive exons, a cassette exon and an alternative 3' splice site^{6,21} (**Fig. 1a**). A2BP1 is upregulated in muscle and brain (**Fig. 1b**). The four alternative 5' exons of transcript NM_018723 were detected in brain, and the 5' exon found in transcript NM_145893 was detected in muscle. Within the coding region, brain cells preferentially include the mutually exclusive exon found in NM_018723, whereas skeletal muscle cells include the NM_145893 form. Across all tissues, A2BP1 gene expression is highest in heart, skeletal muscle and the nervous system (**Fig. 1c**). The first (5') mutually exclusive exon is expressed in nervous-system tissues while the second (3') mutually exclusive exon is found in heart and skeletal muscle. Expression of the gene, the first mutually exclusive exon and the second mutually exclusive exon can be combined to estimate the relative abundance of each form across the tissue panel (**Fig. 1c**, right; Methods). Of the two forms represented by the mutually exclusive exons, brain has a higher proportion of form NM_018723.

9,516 splice events are differentially expressed

Across the 48 tissue compendium, 9,516 alternative splicing events were significantly differentially expressed in at least one tissue (Methods and **Supplementary Fig. 2**), similar to the total number of differentially expressed genes (11,700). Of the monitored cassette exons, 42% were differentially expressed in at least one tissue (**Fig. 2a**); a much lower fraction (26%) of monitored alternative 3' splice sites and a higher proportion (55%) of monitored inserted introns were also differentially expressed. The samples with the highest number of differentially expressed alternative splicing events (**Fig. 2b**) relative to the pool include the cell lines HeLa and HCT116, peripheral leukocytes, fetal brain, testis, mammary gland, and skeletal muscle, whereas the samples with the fewest include adipose, adrenal gland and fetal lung. These rankings parallel those for gene expression; that is, the same samples types were among those with the most and fewest differentially expressed genes.

Cassette exon inclusion and exclusion rates varied among the samples (**Fig. 2c**). The ratio between the number of cassette exons differentially included to the number excluded was highest for SW480, breast and lung tumor, retina and brain samples excluding medulla

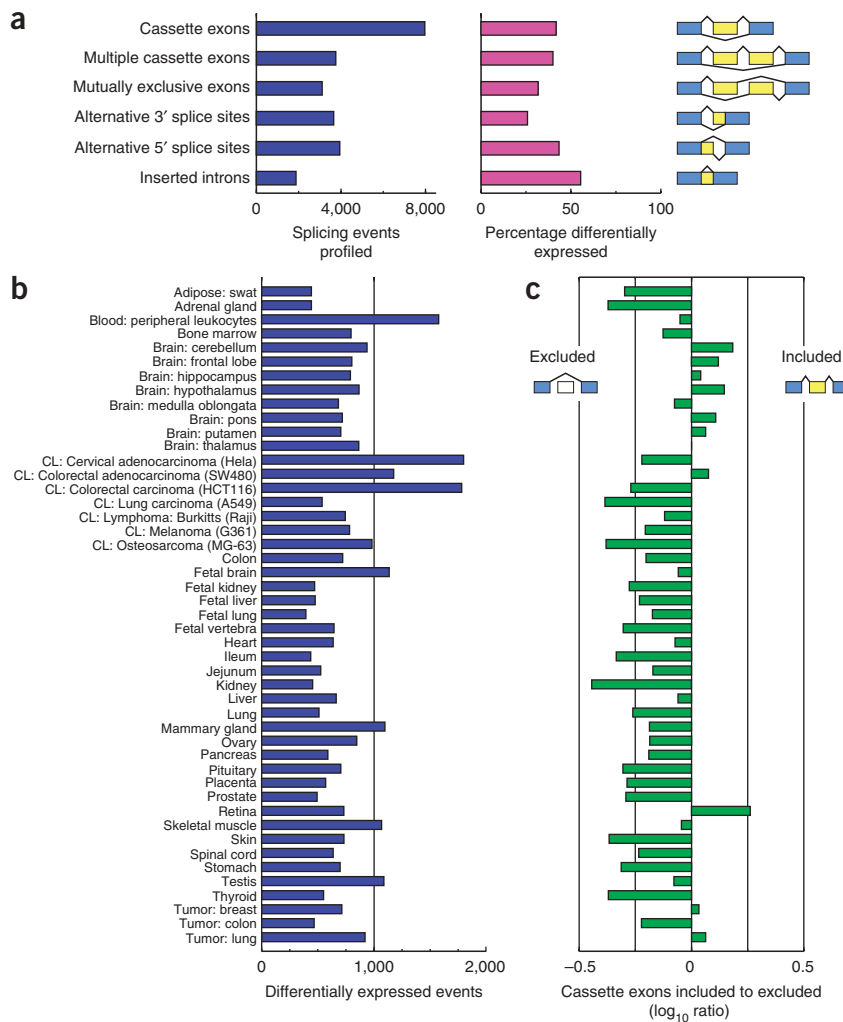


Figure 2 Alternative splicing characteristics. **(a)** The number of events monitored on the arrays and the percentage of each type differentially expressed in at least one tissue. **(b)** The number of events differentially expressed in each tissue. **(c)** The \log_{10} ratio of the number of cassette exons differentially included to those differentially excluded.

oblongata. To test whether this result might be due to the composition of the reference pool (normal adult tissues), we re-ratioed to each individual sample and to the average of all 48 samples, generating 49 *in silico* reference pools (Methods), and computed inclusion rates, exclusion rates and ratios. Although the number of cassette exons included or excluded depended on the reference sample, the inclusion-to-exclusion rankings of samples were similar regardless of the pool, with retina and certain brain, tumor and cell lines consistently ranking highest. These results agree with previous findings that brain tissues express the greatest number of tissue-specific exons¹⁹.

To provide an estimate of the accuracy of the quantitative predictions made by the splicing arrays and analysis tools as part of a larger study (T.A.C., unpublished data), we tested a sample of 23 predictions by semiquantitative RT-PCR and found that 74% of the splice events called differentially expressed by the microarray at P value < 0.1 show changes by PCR of at least 15% in differential expression, and correlations between the microarray and RT-PCR splice event proportionalities of $r = 0.88$ (Methods and **Supplementary Table 1** online).

Transcription and alternative splicing act independently

Similar to previous results¹⁶, we did not detect significant overlap between the differentially expressed genes and the genes with differentially expressed splicing events ($P = 0.4$) in a given tissue. As one specific example, *CLK1* and *CLK2* contain cassette exons whose exclusion generates a protein that dimerizes but inhibits kinase activity²². Here *CLK1* and *CLK2* showed uncorrelated gene expression ($r = 0.13$) across the 48 samples but significantly correlated splicing expression ($r = 0.69$) (**Fig. 3**).

Gene expression correlations are often used to define 'edges' of co-expression networks and infer functional associations. Here gene-gene edges determined from correlated gene expression ($r > 0.75$) and those determined from correlated splice event expression show only 2% overlap (**Supplementary Note** online). Although this overlap is statistically significant, the small overlap demonstrates these are largely different regulatory networks. Finally, we observed that splicing-event expression and gene expression clustered samples similarly but with a few exceptions, such as in lung and breast tumor samples. These cluster with parental tissues (lung and breast) using gene expression but with cell lines using splicing expression, demonstrating that gene expression in these tumor samples is more similar to their normal parental tissues whereas splicing expression is more similar to cell lines (**Supplementary Note**).

Expression of specific splicing events

Ten alternative splicing profiles are highlighted in the **Supplementary Note**, including several associated with nervous system tissues (*GSK3B*, *MAPT (Tau)*, *APP* and *CACNA1B*), muscle tissues (*MEF2C*, *CAMK2D*, *TPM1* and *TPM2*), splicing (*NOVA1*) and cancer (*FGFR2*).

The human gene *CD44* encodes ten variable exons, one of which, *CD44v6*, is the target of bivatuzumab mertansine, an antibody for individuals with advanced carcinoma²³ that was discontinued because

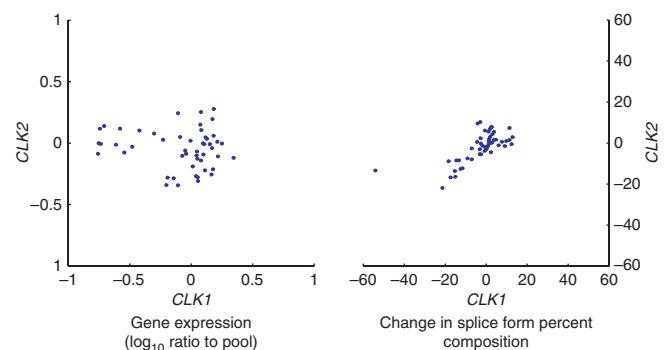


Figure 3 *CLK1* and *CLK2* gene (left) and splice event expression (right).

of skin toxicity in phase I trials²⁴. Although in our data CD44v6 is upregulated in tumors and cancer cell lines, it is expressed highest in skin, highlighting the potential value of this compendium as a public resource. Most microarray experiments use a probe or probe set near the 3' end of each gene and consequently would not detect the isoform-specific variation of *CD44*.

De novo identification of 143 splicing regulatory elements

We next sought to identify regulatory elements in sequences in and adjacent to the tissue-regulated cassette exons. We extracted nucleotide sequence in eight regions ('neighborhoods') around regulated exons and searched for over- and underrepresented nucleotide 'words' between 4 and 7 nucleotides in size, using neighborhood-specific sequences adjacent to all monitored cassette exons as a background set (Fig. 4a, Methods). Examined neighborhoods were 200 nucleotides in size for intronic regions and 39 nucleotides for exonic regions, and the hypergeometric distribution was used to calculate word-enrichment *P* values. In total, 33.5 million enrichment *P* values were calculated.

Using a single tissue (skeletal muscle) to highlight the results, we observed that 8 of 1,024 pentamers have a Bonferroni-corrected *P* value < 0.01 for enrichment in the 200-nucleotide intronic region upstream of cassette exons that are upregulated in skeletal muscle (Fig. 4a). UCUCU is the most enriched, followed by other pyrimidine motifs. In the 200-nucleotide intronic region following cassette exons, three of the 4,096 hexamers are significant. Of note, UGCAUG is most enriched, followed by GCAUGU and UGUGUG. No words were significantly enriched or depleted in the intronic region preceding the downstream 3' splice site.

The compendium can also be used to find enrichment of specific motifs across all 48 tissues and cell lines. For example, the motif UCUCU, which has been associated with *PTB*³⁻⁵, is enriched in the intronic region preceding upregulated cassette exons in brain (*P* value < 10⁻²⁶ in cerebellum), spinal cord, retina, heart and skeletal muscle (Fig. 4b,c). In this dataset, *PTBP1* gene expression shows a marked anticorrelation with UCUCU enrichment, corroborating the inhibitory role of *PTBP1*. The UGCAUG motif, associated with the genes encoding Fox proteins A2BP1 and RBM9 (ref. 6), is enriched in the intronic region following upregulated cassette exons in skeletal muscle (*P* value < 10⁻¹⁶) and heart, with limited enrichment in other tissues, including brain, adipose and colon. *A2BP1* expression correlates highly with UGCAUG enrichment, corroborating the splicing enhancer role of A2BP1. Finally, although we showed above that muscular and neuronal tissues express different A2BP1

isoforms, we observed UGCAUG enrichment in both tissues, although it was highest in muscle and heart.

The systematic analysis of all words in all samples and in all neighborhoods identified 143 significant motifs (*P* < 1 × 10⁻³, Bonferroni-corrected; Methods). Two prominent motifs exist upstream of cassette exons (Fig. 5). A UC-rich cluster, exemplified by UCUCU, is most enriched in brain and muscle tissues, and the AG-rich cluster, including GAGG, AGAGG and AGGG, is depleted in cassette exons upregulated in brain. Other clusters are enriched in brain (UGCUCU) and in several tissues (UGCAUG). Smaller clusters include motifs AGAA, CGCCU and UGAA.

Motifs in the intronic neighborhood following upregulated cassette exons cluster into five groups (Fig. 6). UGUGUG is enriched in

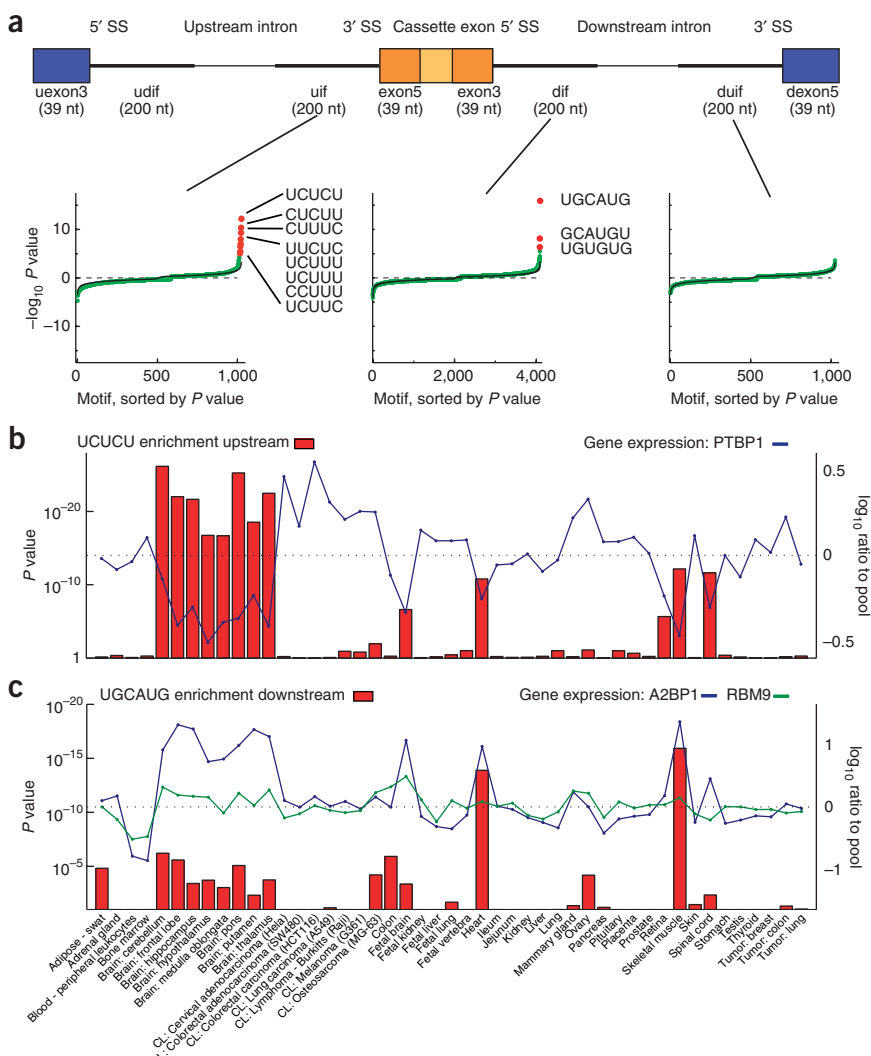


Figure 4 Motif identification and enrichment. (a) Identification of alternative splicing motifs enriched in eight regions adjacent cassette exons upregulated in skeletal muscle. exon5 (exon3), 5' (3') portion of cassette exons; uif (dif), intronic fraction upstream (downstream); uexon3 (dexon5) and udif (duif) are the corresponding regions adjacent the upstream (downstream) exons. Sorted pentamer and hexamer enrichment in three exemplary regions are shown. Green points are $-\log_{10} P$ values; magenta points are those with a Bonferroni-corrected *P* value less than 0.01. Positive (negative) *P* values indicate motif enrichment (depletion). The black line represents the average of 200 randomized runs. (b) Enrichment of UCUCU in human tissues and cell lines. Left axis: enrichment of UCUCU in the 200 nt upstream of upregulated cassette exons. Right axis: gene expression of *PTBP1*. (c) Enrichment of UGCAUG. Left axis: enrichment of UGCAUG in the 200 nt downstream of upregulated cassette exons. Right axis: gene expression of Fox proteins A2BP1 and RBM9. *P* values shown are not Bonferroni corrected.



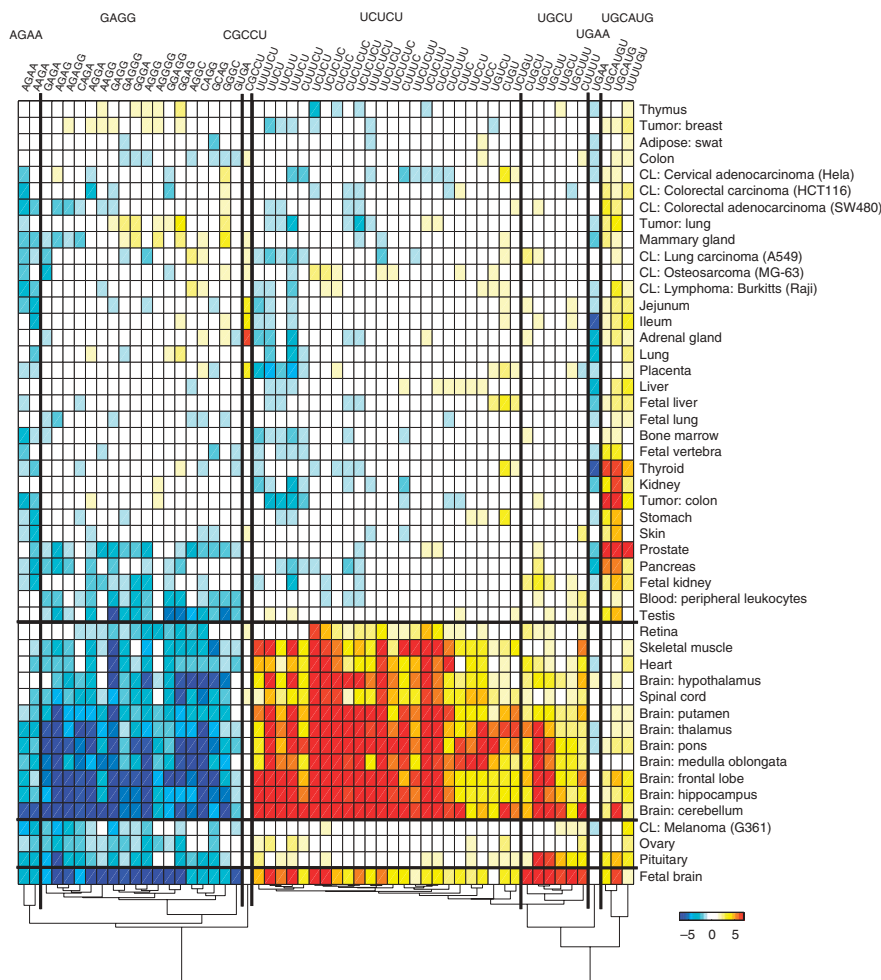


Figure 5 Motif enrichment upstream of cassette exons upregulated in human tissues and cell lines. Values ($-\log_{10} e$ value) are positive for enrichment and negative for depletion. Motifs and tissues are clustered using agglomerative clustering.

muscle and brain subsections, UGCAUG is enriched primarily in heart and skeletal muscle and UUUU is enriched in brain tissues. AG-rich motifs are depleted downstream of cassette exons upregulated in several tissues, including brain, peripheral leukocytes, bone marrow and striated muscle. UACUA is enriched in hypothalamus.

Enrichment occurs in only two other neighborhood and regulation combinations. Immediately upstream of downregulated cassette exons, UCUCU enrichment occurs in all samples except brain, spinal cord, muscle, heart and leukocytes. Coupled with *PTBP1* gene expression, these data corroborate the role of PTB in silencing downstream exons. In the intron downstream of the exon preceding upregulated cassette exons (the 5' splice site), AU-rich motif enrichment occurs in brain and G-rich motif enrichment occurs in HeLa and HCT116, whereas G-rich motif depletion occurs in brain. G-rich motifs are highly enriched at the 5' splice site preceding cassette exons relative to constitutive exons. G-rich motifs may act to silence cassette exons in brain when positioned in the 5' splice site following a cassette exon and may be a generic 5' splice-site defining factor^{8,9}. This suggests a similar role for G-rich motifs near the 5' splice-site upstream of cassette exons.

This set of predicted alternative splicing motifs is in agreement with existing studies, including tissue-specific roles for UGUGU, UCUUU, UGCAUG, UGUGUC and UUUUU^{18,25–29}. In other

cases, motifs identified in the literature, such as ACUAAAC^{29,30}, lie just below our threshold of statistical significance. Fagnani *et al.*¹⁷ identified pyrimidine-rich intronic motifs adjacent to brain-enriched cassette exons but with enrichment spread over several genomic regions and with other motifs, such as UGCAUG, scoring lower.

High-resolution map of RNA alternative-splicing regulation

We expected motif enrichment to occur non-uniformly across the neighborhoods, especially within the 200-nucleotide intronic regions. To more precisely predict where individual motifs exert a regulatory impact, we examined each motif's frequency at each nucleotide position in each of the eight neighborhoods, using a Gaussian wavelet for smoothing (Methods).

UGCAUG occurs 10–80 nucleotides following muscle cassette exons

The motif UGCAUG has been associated with Fox proteins⁶. We found UGCAUG enrichment highest in the intronic neighborhood following cassette exons upregulated in striated muscle (Fig. 4c). When examined at higher resolution, the regulatory influence of UGCAUG in muscle varied across and within the eight neighborhoods (Fig. 7). A broad, highly significant enrichment of UGCAUG occurred from 10 to 80 nucleotides downstream of cassette exons upregulated in heart and skeletal muscle. A second enrichment peak occurred from 65 to 15 nucleotides preceding cassette exons downregulated in heart, whereas less enrichment occurred in

skeletal muscle in this region. Using RT-PCR, RNAi and cDNA overexpression, we validated the position-specific influence of UGCAUG on cassette exon inclusion, identified Fox alternative-splicing targets and found that the targets are enriched for genes involved in neuromuscular function³¹.

UCUCU occurs 110–35 nucleotides preceding regulated cassette exons

UCUCU has been associated with PTB proteins^{3–5}. The motif UCUCU frequently occurs directly upstream of 3' splice sites as part of the polypyrimidine tract. Indeed, when we examined constitutive and cassette exons, both showed high UCUCU occurrence at the 3' splice site relative to the average intronic rate. However, enrichment upstream of constitutive exons extended only 35 nucleotides from the 3' splice site into the upstream intron, whereas tissue-varying cassette exons showed extended enrichment (Fig. 8a). Exons upregulated in cerebellum showed marked UCUCU enrichment from –95 to –15 nucleotides (Fig. 8a). Fetal kidney showed UCUCU enrichment in a similar location, from –75 to –20 nucleotides, although this enrichment surrounded downregulated cassette exons. Almost every tissue showed UCUCU enrichment in a similar location, from –110 to –35 nucleotides preceding cassette exons (Fig. 8b). To our knowledge, this is the first high-resolution map of UCUCU location and splice

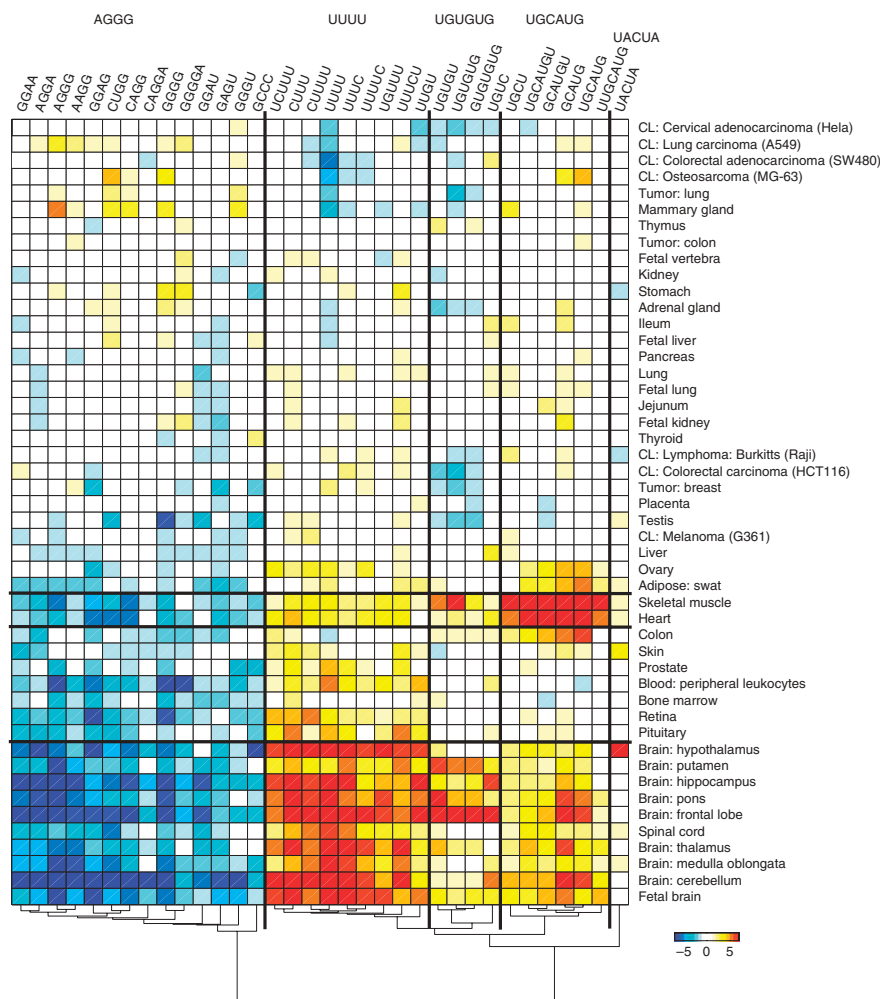


Figure 6 Motif enrichment downstream of cassette exons upregulated in human tissues and cell lines. Values ($-\log_{10}$ e value) are positive for enrichment and negative for depletion. Motifs and tissues are clustered using agglomerative clustering.

regulatory influence. Brain tissues, spinal cord, retina and striated muscle showed enrichment preceding upregulated cassette exons, whereas other samples showed enrichment preceding downregulated cassette exons. Thus, we find that UCUCU enrichment occurs in the polypyrimidine tract immediately preceding the 3' splice site upstream of all exons, but enrichment from -110 to -35 nucleotides occurs only upstream of tissue-regulated cassette exons.

Exonic splicing elements act to define exons (see ref. 32–34 for examples). Although we examined both introns and exons for motifs associated with tissue-varying cassette exons, only intronic motifs passed the P -value cutoff. This might suggest that intronic motifs have a greater role in tissue-specific cassette exon regulation, but we searched only 39 nucleotides of each exonic region compared to 200 nucleotides for each intronic region, and the smaller window lessens the computed significance of exonic motifs. Indeed, we see evidence for exonic UCUCU enrichment at the 3' edge of cassette exons expressed at higher levels in brain and heart but at less significant P values (Fig. 8b). We also did not build cross-species conservation into our statistical model for motif detection. To assess whether more complex motif-detection methods would significantly alter our results, we tested several other published methods, both pre-filtering sequences using cross-species conservation (for example, ref. 35), and filtering

motifs based on frequency in neighborhoods adjacent to alternate and constitutive exons (for example, ref. 36). The results were largely similar in terms of the motifs identified, associated samples and associated locations (Supplementary Note). For example, the P value for UGCUAG enrichment downstream of skeletal muscle enriched exons changed from 1×10^{-16} to 1×10^{-12} when using conservation and is still the most significant word. The next enriched word in both cases is the related word GCAUGU at 1×10^{-9} and 1×10^{-7} , respectively. Exonic motifs remain below significance.

UGCU, UGUGU and AG-rich motifs show different localization

Other previously established relationships between RNA-binding proteins and motifs include muscleblind proteins binding UGCU¹⁰, and CELF¹² and SUP-12 (RBM38)^{12,13} proteins interacting with UGUGU. Here UGCU enrichment occurs upstream of cassette exons upregulated in brain, from -100 to -5 nucleotides upstream of the 3' splice site. Less significant enrichment is found 5–50 nucleotides downstream of brain-upregulated cassette exons. Skeletal muscle and heart show enrichment 30–110 nucleotides following upregulated cassette exons but not upstream. UGUGU shows consistent enrichment 10–100 nucleotides following brain and spinal cord upregulated cassettes. hnRNP A/B and hnRNP F/H bind purine-rich motifs GGGG and AGGGG, respectively^{8,9}. In our data, AGGG and similar purine motifs are depleted preceding brain upregulated cassette exons (Fig. 5). When examined at higher resolution, depletion of

AG-rich motifs occurs over a wide region. In cerebellum, the depletion ranges from 150 nucleotides preceding the cassette exon to over 100 nucleotides beyond the exon.

FOX and PTB act on nonoverlapping sets of cassette exons

As both the UCUCU and UGCAUG words seem to regulate alternative splicing in some of the same samples, but only when positioned in precise regions around exons, we explored whether they occur around the same cassette exons. In cassette exons upregulated in skeletal muscle, we counted occurrences of UCUCU in the region -110 to -35 nucleotides upstream of the cassette exon and UGCAUG in the region from 10 to 80 nucleotides downstream of the cassette exon (Supplementary Fig. 3 online). At least one of the motifs occurs adjacent to 33% of cassette exons upregulated in skeletal muscle. However, they co-occur adjacent to only 2% of the exons, not significantly below the 3% expected by chance ($P = 0.2$), suggesting these two motifs, both enriched in muscle, represent independent regulatory mechanisms. In cerebellum, as in skeletal muscle, UGCAUG and UCUCU are both associated with upregulated cassette exons. We found that 10% and 23% of the cassette exons upregulated in cerebellum contain the motif in the identified region, respectively, and 31% of the exons contain at least one motif. The motifs co-occur

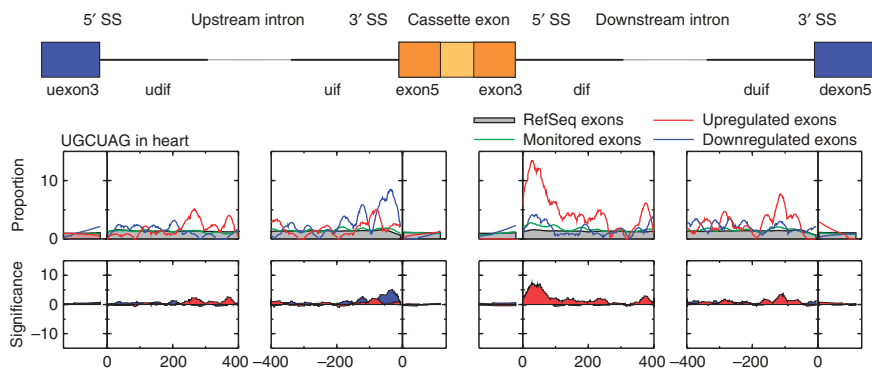


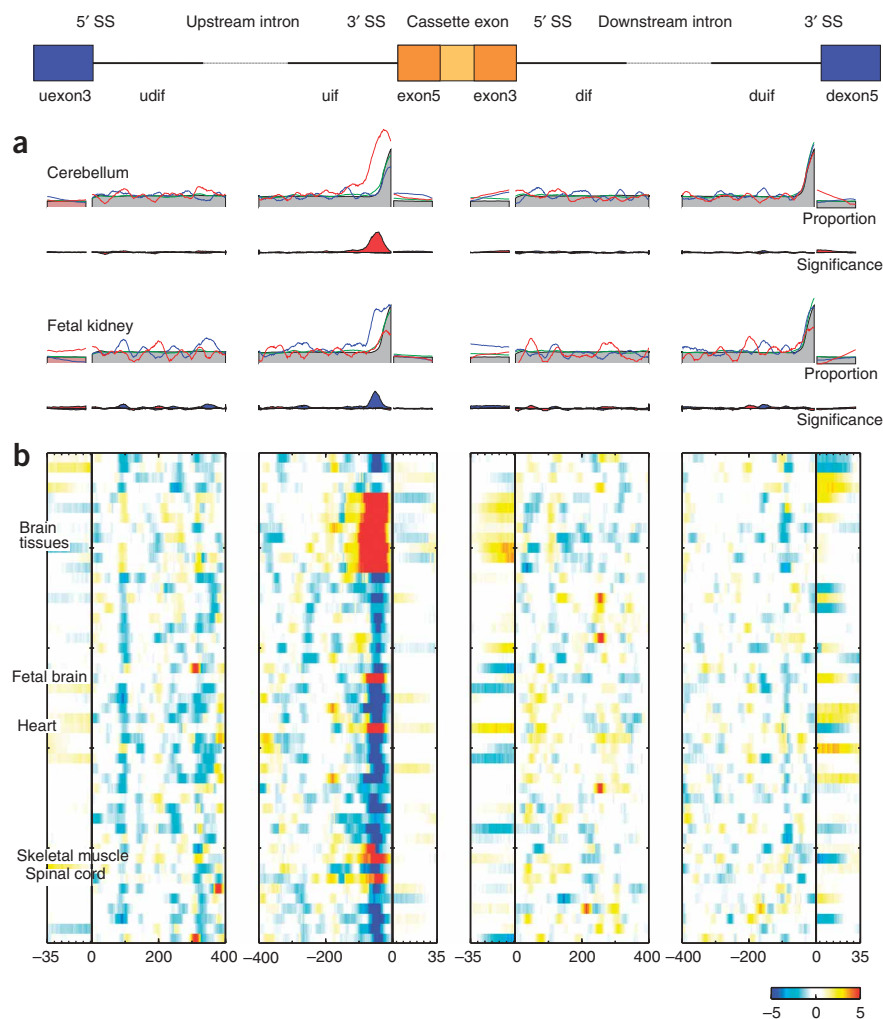
Figure 7 Higher-resolution enrichment of UGCAUG adjacent heart-regulated cassette exons. Middle: smoothed fraction of the cassette exons with UGCAUG. Red, heart upregulated cassette exons; blue, heart downregulated; green, all monitored exons; filled gray regions, RefSeq exons. Bottom: hypergeometric probability ($-\log_{10} P$ value) for up- and downregulated exons relative to all monitored exons.

adjacent only 2% of the exons, the percentage expected by chance, suggesting independent action as in skeletal muscle. In fetal kidney, on the other hand, UGCUAG is not enriched adjacent to up- or downregulated cassette exons, likely reflecting the lower levels of Fox-1 expression, whereas UCUCU enrichment occurs upstream of downregulated cassette exons, likely reflecting higher levels of PTB expression.

Predicted relationships of RNA-binding proteins and motifs

The large number of samples and splicing events in the compendium can be leveraged to predict associations between *trans*-acting splicing regulatory proteins and binding elements. For 135 of the motifs identified (Figs. 5 and 6), we calculated a signed, normalized rank-order metric representing the similarity between the motif enrichment or depletion (P value) tissue profiles and the gene expression profiles of RNA-binding proteins (Supplementary Figs. 4 and 5 online and Methods). The results of this calculation represent *de novo* predictions of potential protein-motif partners and capture many known relationships. PTBPI has the highest absolute score, with a negative

Figure 8 Higher-resolution enrichment of UCUCU adjacent regulated cassette exons. (a) Smoothed fraction of the cassette exons with UGCAUG in cerebellum (upper) and fetal kidney (lower). Red, upregulated cassette exons; blue, downregulated; green, all monitored exons; filled gray regions, RefSeq exons. Maximum significance in cerebellum/uif is P value $< 1 \times 10^{-22}$; maximum proportion is 52. Colors are as in Figure 7 (b) Hypergeometric probability ($-\log_{10} P$ value) for up- and downregulated exons relative to all monitored exons. At each point, the most significant P value associated with either up- or downregulated exons is shown. Samples are ordered alphabetically as in Figure 2.



value for UCUCU upstream of cassette exons and a negative association also with pyrimidine-rich motifs downstream of upregulated cassette exons, as previously established^{4,37}. Upstream of upregulated exons, UCUCU is enriched when PTBPI expression is low but not when it is high. Upstream of downregulated exons, UCUCU is more often enriched when PTBPI is expressed. Thus, cassette exons preceded by UCUCU are downregulated when PTBPI is expressed and upregulated when PTBPI is absent. Upstream of cassette exons, HNRPF has the highest positive score for the purine motif AGGG, and HNRPF and HNRPH1 are known to interact with AG-rich and G-motifs^{8,9}. Downstream of cassette exons, the CELF protein CUGBP2 ranks highest for exon inclusion using UGUGUG, and Fox proteins A2BP1 and

RBM9 rank first and second, respectively, for UGCAUG. SFRS6, SFRS7 and HNRPF score positively for AGGG. The fact that expression of Fox, CELF and HNRPF are positively associated with their motifs surrounding upregulated cassette exons implies that the exons are preferentially included when the protein is

expressed, and suggests a mechanism where the protein acts to enhance inclusion of exons that are otherwise skipped.

The RNA-binding protein NOVA1 targets YCATY and YCAY motifs, with a position-dependent influence^{38,39}. We examined our data for this degenerate motif, summing the values for all four words of YCATY (CCATC, CCATT, TCATC, TCATT) and calculating the hypergeometric probability against the count of the similar set of words in the background. Exons downregulated in brain are enriched in YCATY upstream, whereas exons upregulated in brain are depleted of YCATY upstream and enriched downstream (**Supplementary Fig. 6** online). We observed NOVA1 levels almost tenfold higher than the pool in brain and spinal cord, corroborating a regulatory mechanism in which NOVA1 expression causes exon skipping when bound to upstream YCATY and exon inclusion when bound to YCATY downstream of the exon. These results are fully consistent with previous reports on the position-specific role of NOVA1 (ref. 39).

DISCUSSION

This is the first genome-scale compendium of human alternative splicing events and the largest alternative splicing–event compendium of any species, with each isoform of 24,426 splicing events measured in 48 tissues and cell lines. These data provide a resource for further studies of the expression and regulation of the transcriptome with detail not available previously. We also provide a catalog of annotated splicing events; the mapping of all probes to the hg18 human genome, viewable in the UCSC browser; and the expression of each probe, gene, exon, splicing event and all word enrichments in each tissue. Although not investigated here, these data will be of substantial value in mapping and analyzing alternative 5' and 3' exon usage and tissue-specific alternative polyadenylation.

The splicing event expression compendium was then used to identify candidate regulatory motifs, identifying 143 motifs in five main groups that are associated with tissue-varying alternative splicing. For each motif, we measured the enrichment in each tissue and neighborhood combination and determined the regulatory impact (inclusion or exclusion) on the associated cassette exon. In cerebellum, for example, over 30% of the preferentially included cassette exons are adjacent to either a PTB (–110 to –35 nucleotides upstream) or Fox (10 to 80 nucleotides downstream) motif.

Our results extend previous studies of motifs in brain and muscle to 48 diverse samples, and present tissue- and position-specific maps of each motif's likely regulatory influence at a resolution that to our knowledge is only currently available for YCAY (Nova)³⁹. With the more precise location of motif regulatory impact, we are able to show that co-occurrence rate of the UGCAUG (Fox) and UCUCU (PTB) motifs around tissue-regulated cassette exons is similar to that expected by chance, suggesting that they act independently.

Finally, we used splicing array data to identify RNA regulatory motifs and predict binding elements for RNA-binding proteins *de novo*. Although these predictions will require further validation, the fact that many established associations rank highly (for example, UGCAUG with Fox-1, UCUCU with PTB1 and UGUGUG with CELF) suggests that these results could be used as part of a prioritization scheme for further experimentation.

METHODS

Microarray pattern generation. We downloaded genome and transcript sequences from the National Center for Biotechnology Information on January 8, 2003. We aligned RefSeq, mRNA, EST⁴⁰ and patent transcripts to the genome using sim4 (ref. 41) and identified all exons and exon–exon junctions. We also

aligned mouse transcripts to the human genome to identify possible splice forms not yet present in human transcript databases⁴². An optimized 60-nucleotide probe was designed to monitor each exon and a 36-nucleotide probe was centered across each exon–exon junction⁴³. Exons less than 60 nucleotides were monitored using shorter probes attached to T-stilts. Probes predicted to perform poorly, such as those associated with repeat sequences or containing unacceptable GC content, were discarded. In total, 383,014 oligonucleotide probes to monitor 203,672 exons and 178,351 exon–exon junctions in 17,939 genes were synthesized to a 17 array set, with each array containing 23,107 noncontrol probes. Arrays were ordered from Agilent. Probes have been mapped to the hg18 genome and can be viewed with the UCSC genome browser using the supplementary probe alignment file (see URLs section below).

Tissue preparation and hybridization. We hybridized 48 diverse human tissues and cell lines to this array set. Samples were purchased as pools from multiple donors, typically over ten (Clontech). We isolated poly(A)+ RNA from each sample, amplified and labeled the entire transcript structure with Cy3 and Cy5 (ref. 43) and hybridized all samples against a common reference pool in a dye-swamp replicate experiment⁴⁴. Pooled RNA from 20 diverse disease-free adult tissue pools comprised the reference pool. Single array intensities were normalized spatially and for overall intensity; fluor-reverse pairs were combined; and intensity, relative change (\log_{10} ratio) and uncertainty values were output for each probe and sample⁴⁵. Tissue-specific probe intensities were further normalized by the pool intensity for the specific probe, relative to the average intensity of the pool for the probe when hybridized against other samples.

Gene expression. We determined gene expression by averaging values from three selected probes per gene. Probes were prioritized by location in constitutively transcribed exons or junctions and then by correlation with the average of all constitutive-element-monitoring probes across the 48 samples. From the three probes, \log_{10} expression ratios represent the error-weighted average ratio to the pool and intensities as the average probe intensity. *P* values are assigned to relative expression values using the uncertainty and reflect the probability of no differential expression between the sample and the pool.

Alternative splicing event profiling. We identified putative mutually exclusive alternative splicing events found in our alignment of RefSeq, GenBank, dbEST, patent and mouse transcripts to the human build 35 version 1 genome assembly⁴⁶. As per the microarray design process, transcripts were aligned to the genome, and exon and exon–exon junction coordinates were identified. For each gene, we examined the exon and junction coordinates for mutually exclusive splicing events, including cassette exons (single and multiple), mutually exclusive exons, alternative 5' and 3' splice sites, and retained introns. The exon and junction nucleotide sequence specific to each form was extracted; probes were associated with each form on the basis of sequence identity.

For alternative splicing events for which both inclusion and exclusion were monitored, we calculated a relative change (\log_{10} ratio) to the reference pool and intensity for each form. If multiple probes reported on a form, we combined \log_{10} ratios using error-weighted averaging and calculated a median intensity. To estimate the proportion of a given splice form relative to the pool, we used “method 1 + 2” of Ule *et al.*¹⁴, similar to a method described by Fehlbauer *et al.*⁴⁷. For a given alternative splicing event, log ratios monitoring event inclusion and exclusion were normalized by gene expression to isolate splicing changes from transcription changes. We then compared these normalized inclusion and exclusion log ratios. The output is a measure of the change in percentage of one splice form, such that a change from 80% of total to 20% of total is reported as –60. If no change in alternative splicing occurs, the method is unable to assign proportionality.

Error estimate and significance calls for differential splice expression. We added an uncertainty, *P* value and filtering to the alternative splicing–event profiling. We flagged events for which the gene intensities were below the noise level in either sample, for which the event intensities were below the noise level in both samples, or for which either the gene or event intensities were near saturation levels in either sample. We also flagged events showing intensity more than tenfold higher than the gene intensity, as this represents possible

cross-hybridization. In true cases of differential alternative splicing, the \log_{10} ratios monitoring the splice event inclusion and exclusion should have opposite signals after removal of the gene expression changes; we therefore flagged those not consistent. Using standard error propagation⁴⁸, we calculated an uncertainty with each log ratio measurement and a *P* value for each splicing event, representing the probability that the splicing event is not differentially expressed after accounting for gene expression changes. We considered splice events with a change of at least magnitude 5, a *P* value less than 0.3 and no flags as significantly differentially expressed.

Validation of splicing event profiling. In conjunction with the Cooper laboratory (Baylor), we established validation rates for this platform. We profiled mouse heart at different development stages (T.A.C., unpublished data). We tested 23 microarray predictions (with *P* value < 0.1 and passing the intensity and cross-hybridization filters described above) and found that 17 (74%) showed RT-PCR-determined proportionality changes exceeding 15 percentage points (for example, isoform A changes from 60% to 45% of the total) and the correlation between microarray and RT-PCR splice event profiles was $r = 0.88$ (Supplementary Table 1).

Re-ratio of microarray data. The microarray values were derived from two-color hybridizations of the sample and a common reference pool. For each sample, the resultant values included an intensity, \log_{10} ratio to pool, and \log_{10} ratio-to-pool uncertainty. To define a different pool *in silico* using one of the existing samples, the \log_{10} ratio to 'new pool' was calculated for each sample as the difference between the \log_{10} ratio to pools from the sample and from the new pool sample. The \log_{10} ratio to 'new pool' uncertainty was calculated as the square root of the sum of the squares of each \log_{10} ratio-to-pool uncertainty.

Motif identification. For each tissue, we identified up- and downregulated cassette exons and searched associated genomic regions for over- and under-represented motifs. Up- and downregulated cassette exons were identified that passed the described intensity and consistency filters and showed a minimum percent inclusion change of 5 and a *P* value lower than 0.3. For each cassette exon, we extracted the repeat-masked nucleotide sequence in eight regions, including the 3' edge of the previous exon, the intronic region adjacent the upstream 5' splice site, the intronic region adjacent the upstream 3' splice site, the 5' region of the cassette exon, the 3' region of the cassette exon, the intronic region adjacent the downstream 5' splice site, the intronic region adjacent the downstream 3' splice site and the 5' edge of the following exon. For intronic and exonic regions, we extracted 200 nucleotides and 39 nucleotides, respectively, based on previous studies^{18,39,49} and required introns to be at least 300 nucleotides to limit the impact of neighboring splice sites.

The neighborhood-specific background set included sequences from the set of cassette exons monitored on the microarrays. For each neighborhood in each tissue, we counted the occurrence of every word, size 3 through 7. Then, for each word, tissue and region, we used the cumulative hypergeometric distribution to assign a *P* value representing the probability for observing that number of occurrences in the foreground versus the number in the background set. In cases where we examined enrichment (inverse cumulative hypergeometric) and depletion (cumulative hypergeometric), the most significant *P* value was retained and a sign, positive or negative, was assigned to the *P* value depending on whether enrichment or depletion, respectively, was most significant. Counting the number of motifs, rather than the number of cassette exons with the motif, was more sensitive for motifs that commonly occur in a given region, such as UCUCU upstream of cassette exons.

To identify motifs, such as those in plotted Figure 5, we identified words with signed hypergeometric *P* values more significant than 1×10^{-3} (Bonferroni corrected) in any tissue in the specific neighborhood, minus words found in longer words with more significant *P* values. Using randomized exon annotations, we calculated a false-discovery rate (FDR) for each motif in each neighborhood. UUUUU and AAAAA had significantly higher FDRs and were excluded from further analysis.

For the high-resolution enrichment study, the number of motifs at each position was convolved with a Gaussian wavelet. The Gaussian wavelet was width 40, with maximum value of 1 at position zero, falling to 0.26 at ± 20 . The smoothed counts were calculated at each position for tissue-upregulated

cassette exons, tissue-downregulated cassette exons and the background sets. We again used the hypergeometric distribution to calculate *P* values for enrichment and depletion from the smoothed motif counts, in both tissue-upregulated and tissue-downregulated sets, versus the corresponding motif counts from the set of all cassette exons monitored.

Co-regulation of motifs and RNA-binding protein transcript expression. We considered RNA-binding proteins found in the Panther mRNA splicing gene set and those classified by Interpro as having a RNP domain. Muscleblind proteins (for example, MBNL2) are not included in these sets; they are found in 24 genes in the Panther double-stranded DNA binding set, so we included this set as well. For each significant motif in each genomic region, we calculated a nonparametric score by sorting tissue enrichment rankings on the basis of the gene expression rankings for each protein and identifying the greatest divergence from random. The maximum value for each motif was normalized to 1. We preserved the sign to represent positive and negative divergence. Clustering in figures is agglomerative clustering.

URLs. Compendium of alternative splicing expression, gene expression, probe and splicing event nucleotide sequences, genome browser tracks, and individual splicing event figures: http://rulai.cshl.edu/Rosetta_AS_supp/ and <http://rulai.cshl.edu/dbCASE>.

Accession codes. NCBI GEO: microarray data have been deposited with accession code GSE11863. GenBank: *CLK1*, NM_004071; *CLK2*, NM_003993; *A2BP1*, NM_018723 and NM_145893.

Note: Supplementary information is available on the Nature Genetics website.

ACKNOWLEDGMENTS

We thank C. Armour, C. Raymond, D. Haynor, V. Emilsson, P. Garrett-Engle, F. Roth, P. Loerch, R. Chen, C. Rohl, M. Tompa, E. Schadt and L. Lim for input, Rosetta's Gene Expression Laboratory microarray hybridization facility for microarray data, and S. Carlson for project management. Funding for T.A.C. provided by R01GM076493.

AUTHOR CONTRIBUTIONS

J.M.J. conceived the experiment; J.C.C. and J.M.J. executed the experiment and wrote the paper; J.C.C. designed the microarrays and analyzed the data; J.C.C. and C.Z. identified motifs; J.K.S. and A.V.K. processed and managed data; and A.K. and T.A.C. provided validation experiments.

Published online at <http://www.nature.com/naturegenetics/>

Reprints and permissions information is available online at <http://npg.nature.com/reprintsandpermissions/>

- Johnson, J.M. *et al.* Genome-wide survey of human alternative pre-mRNA splicing with exon junction microarrays. *Science* **302**, 2141–2144 (2003).
- Kwan, T. *et al.* Genome-wide analysis of transcript isoform variation in humans. *Nat. Genet.* **40**, 225–231 (2008).
- Chan, R.C. & Black, D.L. Conserved intron elements repress splicing of a neuron-specific c-src exon *in vitro*. *Mol. Cell. Biol.* **15**, 6377–6385 (1995).
- Singh, R., Valcarcel, J. & Green, M.R. Distinct binding specificities and functions of higher eukaryotic polypyrimidine tract-binding proteins. *Science* **268**, 1173–1176 (1995).
- Gooding, C., Roberts, G.C. & Smith, C.W. Role of an inhibitory pyrimidine element and polypyrimidine tract binding protein in repression of a regulated alpha-tropomyosin exon. *RNA* **4**, 85–100 (1998).
- Underwood, J.G., Boutz, P.L., Dougherty, J.D., Stoilov, P. & Black, D.L. Homologues of the *Caenorhabditis elegans* Fox-1 protein are neuronal splicing regulators in mammals. *Mol. Cell. Biol.* **25**, 10005–10016 (2005).
- Minovitsky, S., Gee, S.L., Schokrpur, S., Dubchak, I. & Conboy, J.G. The splicing regulatory element, UGCAUG, is phylogenetically and spatially conserved in introns that flank tissue-specific alternative exons. *Nucleic Acids Res.* **33**, 714–724 (2005).
- Martinez-Contreras, R. *et al.* Intronic binding sites for hnRNP A/B and hnRNP F/H proteins stimulate pre-mRNA splicing. *PLoS Biol.* **4**, e21 (2006).
- Han, K., Yeo, G., An, P., Burge, C.B. & Grabowski, P.J. A combinatorial code for splicing silencing: UAGG and GGGG motifs. *PLoS Biol.* **3**, e158 (2005).
- Ho, T.H. *et al.* Muscleblind proteins regulate alternative splicing. *EMBO J.* **23**, 3103–3112 (2004).
- Forch, P. *et al.* The apoptosis-promoting factor TIA-1 is a regulator of alternative pre-mRNA splicing. *Mol. Cell* **6**, 1089–1098 (2000).

12. Faustino, N.A. & Cooper, T.A. Identification of putative new splicing targets for ETR-3 using sequences identified by systematic evolution of ligands by exponential enrichment. *Mol. Cell. Biol.* **25**, 879–887 (2005).
13. Kuroyanagi, H., Ohno, G., Mitani, S. & Hagiwara, M. The Fox-1 family and SUP-12 coordinately regulate tissue-specific alternative splicing in vivo. *Mol. Cell. Biol.* **27**, 8612–8621 (2007).
14. Ule, J. *et al.* Nova regulates brain-specific splicing to shape the synapse. *Nat. Genet.* **37**, 844–852 (2005).
15. Ule, J. *et al.* CLIP identifies Nova-regulated RNA networks in the brain. *Science* **302**, 1212–1215 (2003).
16. Pan, Q. *et al.* Revealing global regulatory features of mammalian alternative splicing using a quantitative microarray platform. *Mol. Cell* **16**, 929–941 (2004).
17. Fagnani, M. *et al.* Functional coordination of alternative splicing in the mammalian central nervous system. *Genome Biol.* **8**, R108 (2007).
18. Sugnet, C.W. *et al.* Unusual intron conservation near tissue-regulated exons found by splicing microarrays. *PLoS Comput. Biol.* **2**, e4 (2006).
19. Clark, T.A. *et al.* Discovery of tissue-specific exons using comprehensive human exon microarrays. *Genome Biol.* **8**, R64 (2007).
20. Griffith, M. *et al.* ALEXA: a microarray design platform for alternative expression analysis. *Nat. Methods* **5**, 118 (2008).
21. Nakahata, S. & Kawamoto, S. Tissue-dependent isoforms of mammalian Fox-1 homologs are associated with tissue-specific splicing activities. *Nucleic Acids Res.* **33**, 2078–2089 (2005).
22. Duncan, P.I., Stojdl, D.F., Marius, R.M. & Bell, J.C. In vivo regulation of alternative pre-mRNA splicing by the Clk1 protein kinase. *Mol. Cell. Biol.* **17**, 5996–6001 (1997).
23. Rupp, U. *et al.* Safety and pharmacokinetics of bivatuzumab mertansine in patients with CD44v6-positive metastatic breast cancer: final results of a phase I study. *Anticancer Drugs* **18**, 477–485 (2007).
24. Riechelmann, H. *et al.* Phase I trial with the CD44v6-targeting immunoconjugate bivatuzumab mertansine in head and neck squamous cell carcinoma. *Oral Oncol.* **44**, 823–829 (2008).
25. Brudno, M. *et al.* Computational analysis of candidate intron regulatory elements for tissue-specific alternative pre-mRNA splicing. *Nucleic Acids Res.* **29**, 2338–2348 (2001).
26. Yeo, G.W., Van Nostrand, E., Holste, D., Poggio, T. & Burge, C.B. Identification and analysis of alternative splicing events conserved in human and mouse. *Proc. Natl. Acad. Sci. USA* **102**, 2850–2855 (2005).
27. Yeo, G.W., Nostrand, E.L. & Liang, T.Y. Discovery and analysis of evolutionarily conserved intronic splicing regulatory elements. *PLoS Genet.* **3**, e85 (2007).
28. Yeo, G.W. *et al.* Alternative splicing events identified in human embryonic stem cells and neural progenitors. *PLoS Comput. Biol.* **3**, 1951–1967 (2007).
29. Das, D. *et al.* A correlation with exon expression approach to identify cis-regulatory elements for tissue-specific alternative splicing. *Nucleic Acids Res.* **35**, 4845–4857 (2007).
30. Voelker, R.B. & Berglund, J.A. A comprehensive computational characterization of conserved mammalian intronic sequences reveals conserved motifs associated with constitutive and alternative splicing. *Genome Res.* **17**, 1023–1033 (2007).
31. Zhang, C. *et al.* Defining the regulatory network of the tissue-specific splicing factors Fox-1 and Fox-2. *Genes Dev.* **22**, 2550–2563 (2008).
32. Liu, H.X., Zhang, M. & Krainer, A.R. Identification of functional exonic splicing enhancer motifs recognized by individual SR proteins. *Genes Dev.* **12**, 1998–2012 (1998).
33. Fairbrother, W.G., Yeh, R.F., Sharp, P.A. & Burge, C.B. Predictive identification of exonic splicing enhancers in human genes. *Science* **297**, 1007–1013 (2002).
34. Zhang, W. *et al.* The functional landscape of mouse gene expression. *J. Biol.* **3**, 21 (2004).
35. Goren, A. *et al.* Comparative analysis identifies exonic splicing regulatory sequences—The complex definition of enhancers and silencers. *Mol. Cell* **22**, 769–781 (2006).
36. Fairbrother, W.G. *et al.* RESCUE-ESE identifies candidate exonic splicing enhancers in vertebrate exons. *Nucleic Acids Res.* **32**, W187–W190 (2004).
37. Perez, I., Lin, C.H., McAfee, J.G. & Patton, J.G. Mutation of PTB binding sites causes misregulation of alternative 3' splice site selection in vivo. *RNA* **3**, 764–778 (1997).
38. Jensen, K.B., Musunuru, K., Lewis, H.A., Burley, S.K. & Darnell, R.B. The tetranucleotide UCAY directs the specific recognition of RNA by the Nova K-homology 3 domain. *Proc. Natl. Acad. Sci. USA* **97**, 5740–5745 (2000).
39. Ule, J. *et al.* An RNA map predicting Nova-dependent splicing regulation. *Nature* **444**, 580–586 (2006).
40. Wheeler, D.L. *et al.* Database resources of the National Center for Biotechnology Information. *Nucleic Acids Res.* **36**, D13–D21 (2008).
41. Florea, L., Hartzell, G., Zhang, Z., Ruben, G.M. & Miller, W. A computer program for aligning a cDNA sequence with a genomic DNA sequence. *Genome Res.* **8**, 967–974 (1998).
42. Kan, Z., Castle, J., Johnson, J.M. & Tsinoemas, N.F. Detection of novel splice forms in human and mouse using cross-species approach. *Pac. Symp. Biocomput.* **9**, 42–53 (2004).
43. Castle, J. *et al.* Optimization of oligonucleotide arrays and RNA amplification protocols for analysis of transcript structure and alternative splicing. *Genome Biol.* **4**, R66 (2003).
44. Hughes, T.R. *et al.* Expression profiling using microarrays fabricated by an ink-jet oligonucleotide synthesizer. *Nat. Biotechnol.* **19**, 342–347 (2001).
45. Weng, L. *et al.* Rosetta error model for gene expression analysis. *Bioinformatics* **22**, 1111–1121 (2006).
46. International Human Genome Sequencing Consortium. Finishing the euchromatic sequence of the human genome. *Nature* **431**, 931–945 (2004).
47. Fehlbaum, P., Guihal, C., Bracco, L. & Cochet, O. A microarray configuration to quantify expression levels and relative abundance of splice variants. *Nucleic Acids Res.* **33**, e47 (2005).
48. Taylor, J.R. *An Introduction to Error Analysis* 270 (University Science Books, Mill Valley, California, 1982).
49. Fairbrother, W.G., Holste, D., Burge, C.B. & Sharp, P.A. Single nucleotide polymorphism-based validation of exonic splicing enhancers. *PLoS Biol* **2**, E268 (2004).